Analytical extraction of the recombination zone location in organic light-emitting diodes from emission pattern extrema

Ariel Epstein,* Nir Tessler, and Pinchas D. Einziger

Department of Electrical Engineering, Technion-Israel Institute of Technology, Haifa 32000, Israel
*Corresponding author: arielep@tx.technion.ac.il

We present an analytical method for extracting the recombination zone location from emission patterns produced by organic LEDs (OLEDs). The method is based on derivation of the closed-form expressions for OLED-radiated power developed in previous work and formulation of the analytical relations between the emitter position and the pattern extrema. The results are confirmed to be in good agreement with reported optical measurements. The resultant formulae offer insight regarding the dominant physical processes in the device and can be utilized to assess or verify the location of the recombination zone, a very important parameter in the optimization process of OLED efficiency, from standard optical measurements, otherwise a very difficult task to achieve.   © 2010 Optical Society of America

OCIS codes: 000.3860, 250.3680, 230.3670.

Organic LEDs (OLEDs) have been intensively investigated in the past two decades as promising candidates for novel optoelectronic applications, such as thin and flexible displays and low-cost lasers [1,2]. In recent years, a major effort is being made to improve the outcoupling efficiency of the emitted light [3,4]. In the frame of these attempts, it has been shown that the fine details of the device structure, the choice of materials, and the recombination zone location are closely related to the device efficiency [3,5,6]. As direct measurement of the recombination zone location and width is difficult to perform, numerical simulations solving the transport equations in the device, numerical fitting procedures, and cumbersome experimental techniques remain the main options for optimization and verification of these important parameters [7–9].

In this Letter, we present a rigorous analytical formulation of the relations between the emitter location and the emission pattern produced for a general bottom-emitting (BE) OLED structure. Relying on previous work [10], in which an analytical expression for the emission pattern was derived, we obtain a clear and simple relation between the emission pattern extrema and the recombination zone location. The resultant expressions offer a novel method for extracting electrical properties of devices from their optical characteristics. This enables the examination of dominant electrical processes (as well as verification of the recombination zone location), which have a major effect on the device efficiency and far-field angular distribution [3,5,10]. For the sake of simplicity and clarity, we focus on a two-dimensional (2D) canonical configuration excited by impulsive (line) sources instead of using the more realistic three-dimensional (3D) dipole model. However, the essence of the problem and the physical phenomena remain the same, and, as shall be presented, our formulation can be used to accurately obtain the recombination zone location from reported experimental measurements.

We consider a 2D prototype device with five distinct layers, with a line source embedded at a certain plane $z = z'$ and sandwiched between layers (-1) and $(+1)$,

as depicted in Fig. 1 [1,3]. Both TE (denoted by subscript/superscript e) excitations and TM (denoted by subscript/superscript m) excitations are considered. The wavenumber of the nth layer is given as $k_n = \omega \sqrt{\mu_n \varepsilon_n [1 - j\sigma_n/(\omega \varepsilon_n)]} = (\omega/c)(\mathrm{n}_n - j\kappa_n)$, where c, n, and κ denote the velocity of light in vacuum, refractive index, and extinction coefficient, respectively, and ε_n, μ_n, and σ_n are the permittivity, permeability, and conductivity, respectively. We define the 2D space vector, $\vec{\rho} = \rho_t \hat{t} + z\hat{z} = (-\rho \sin\theta)\hat{t} + (\rho \cos\theta)\hat{z}$, where ρ_t and $\hat{t}$ are its transverse coordinate magnitude and direction, and θ is the angle between the z axis and $\vec{\rho}$. A full description of the notations used in our model can be found in [10].

After examining the typical choice of material and exciton ensemble characteristics, we assume the following: (1) the spatial distribution of the exciton ensemble is small compared with the active layer dimensions, i.e., the spatial broadening could be neglected; (2) the coherence length is much smaller than the weak-microcavity optical length, i.e., interference effects due to multiple reflections in the weak microcavity formed between the substrate/air and organic/metal interfaces could be neglected; (3) losses in nonmetallic layers could be neglected; and (4) reflection from the interface between active layer and ITO is negligible. Under these assumptions, the emission pattern of the device is given by [10]
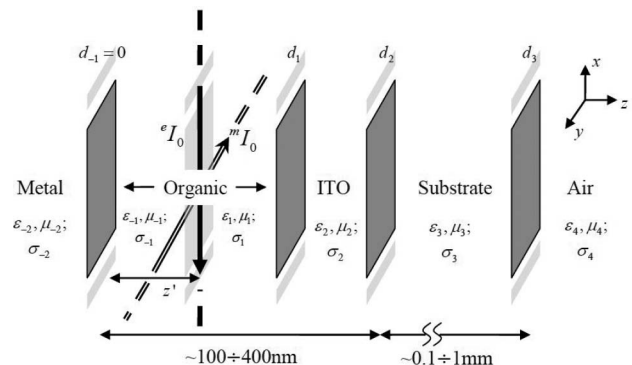
Fig. 1.   Physical configuration of a general 2D BE OLED.

$$S_\rho(\theta) \approx \frac{P_4}{\pi\rho} T_{\mathrm{IS}}(k_t, z') T_{\mathrm{DR}}(k_t) T_{\mathrm{WM}}(k_t) \Big|_{k_t = k_4 \sin\theta}, \quad (1)$$

where we define the simplified image-source, direct-ray, and weak-microcavity transmission factors, respectively, as

$$T_{\mathrm{IS}}(k_t, z') = 1 + |\hat{\Gamma}_{-1}(k_t)|^2$$
$$- 2\mathfrak{R}\{\hat{\Gamma}_{-1}(k_t) e^{-2j\mathfrak{R}\{\beta_1\}(z' - d_{-1})}\}, \quad (2)$$

$$T_{\mathrm{DR}}(k_t) = \prod_{n=3}^{4} |1 + \Gamma_{n-1}(k_t)|^2, \quad (3)$$

$$T_{\mathrm{WM}}(k_t) = \sum_{q=0}^{q_{\max}} \{|\hat{\Gamma}_{-1}(k_t)|^2 |\Gamma_3(k_t)|^2\}^q, \quad (4)$$

where $\Gamma_n(k_t)$ is the forward local reflection coefficient of the nth interface, $n > 0$, given by the Fresnel formula, $\Gamma_n = (1 - \gamma_n)/(1 + \gamma_n)$, where we use the definition of the generalized wavenumber ratio, $_m^e\gamma_n = (k_n/k_{n+1})^{\pm 1} (k_{n+1}/k_n)(\beta_n/\beta_{n+1})$. For the reversed direction, $n < 0$, we define $\hat{\Gamma}_n = -\Gamma_{n-1}$. We use the notation $\vec{k}_t = k_t\hat{t}$ for the transverse wave vector, and $\beta_n = \sqrt{k_n^2 - k_t^2}$ is the wavenumber in the propagation direction $\hat{z}$.

Taking the terms of Eq. (1) to the first order in $|\Gamma_3|$ (substrate/air reflection), neglecting $|\Gamma_2|$ (ITO/substrate reflection), and deriving with respect to $\chi_{\mathrm{air}} = \cos\theta$ (viewing angle) results in the emission pattern extrema conditions, namely,

$$2\phi_{\mathrm{src}}\chi_{\mathrm{act}} + \alpha_{\mathrm{img}} - \alpha_0 = \begin{cases} 2\pi\nu + \pi & \text{local min} \\ 2\pi\nu + \pi - 2\psi_{\mathrm{DR}} & \text{local max} \end{cases}, \quad (5)$$

where $\chi_{\mathrm{act}} = \cos\theta_{\mathrm{act}} = \beta_1/k_1$ denotes the propagation angle in the active layer; $(\alpha_{\mathrm{img}} - \alpha_0)$ is the phase addition due to reflection from the metallic cathode, $\tan{_m^e\alpha_{\mathrm{img}}} = 2\chi_{\mathrm{act}}^{\pm 1} r_{\mathrm{img}}/(1 - \chi_{\mathrm{act}}^{\pm 2} r_{\mathrm{img}}^2)$, $\alpha_0^e = \pi$, and $\alpha_0^m = 0$; and $\phi_{\mathrm{src}} = k_1 z'$ is the phase accumulated by propagation in the active layer from the source to the metal/organic interface at $\theta = 0$. The effect of the direct-ray transmission on the extrema condition is encapsulated in $\tan\psi_{\mathrm{DR}} = (\phi_{\mathrm{src}} + \phi_0)\chi_{\mathrm{DR}}$, where $_m^e\phi_0 = (\pm 1/\chi_{\mathrm{act}}) [\chi_{\mathrm{act}}^{\pm 1} r_{\mathrm{img}}/(1 + \chi_{\mathrm{act}}^{\pm 2} r_{\mathrm{img}}^2)]$, and

$$_m^e\chi_{\mathrm{DR}} = \begin{cases} \dfrac{r_{\mathrm{act}}^2 \chi_{\mathrm{air}}^2}{\chi_{\mathrm{act}}(1 - r_{\mathrm{sub}}\chi_{\mathrm{air}})} \\ \dfrac{r_{\mathrm{act}}^2 \chi_{\mathrm{air}}^2 (r_{\mathrm{sub}} + \chi_{\mathrm{air}})}{r_{\mathrm{sub}}\chi_{\mathrm{act}}(1 - r_{\mathrm{sub}}\chi_{\mathrm{air}}^2)} \end{cases}. \quad (6)$$

Here, $r_{\mathrm{img}} = n_1/\kappa_{-2}$, $r_{\mathrm{act}} = n_4/n_1$, and $r_{\mathrm{sub}} = n_4/n_3$ denote metal/organic, air/organic, and air/substrate wavenumber ratios, respectively. The parameter ν is the solution order, an integer enabling the choice of the appropriate branch of the tangent in Eq. (5). When the source is located close enough to the cathode (with respect to the effective wavelength in the active layer), the

zeroth order solution is applicable. If the active layer is thicker, solutions of higher orders must be taken into account.

Once we establish Eq. (5), the physical interpretation of the extrema condition becomes clear. First, we observe that the angles of local maxima and minima do not depend on the layer dimensions, but only on the emitter location, indicating that the dominant optical process in determining the emission pattern extrema is the image-source interference. This is due to the incoherent nature of the exciton ensemble, which allows us to neglect multiple reflections from the media interfaces [10]. Second, the extrema condition takes the form of a phase-matching condition. The left side of Eq. (5) is the phase accumulated by the ray upon propagation from the source to the cathode and back, and the reflection from the metal/organic interface. For destructive interference (local minima), the right side matches this phase to a full cycle and a half. For constructive interference (local maxima), the phase matching involves a phase shift due to transmission from the active layer to air, which in the limiting case of $T_{\mathrm{DR}} \to 1$ reduces to the familiar Bragg phase-matching condition for constructive interference.

We make use of the Taylor series expansion for $\arctan(\tan\psi_{\mathrm{DR}})$ around $\psi_{\mathrm{DR}} = 0$, $\pi/2$, which allows us to solve Eq. (5) for ϕ_{src} analytically. The resulting solutions are

$$\phi_{\mathrm{src}}^{\min} = \frac{2\pi\nu + \pi - (\alpha_{\mathrm{img}} - \alpha_0)}{2\chi_{\mathrm{act}}} \Big|_{\theta = \theta_{\min}}, \quad (7)$$

$$\phi_{\mathrm{src}}^{\max,<} = \frac{2\pi\nu + \pi - (\alpha_{\mathrm{img}} - \alpha_0) - 2\phi_0\chi_{\mathrm{DR}}}{2(\chi_{\mathrm{act}} + \chi_{\mathrm{DR}})} \Big|_{\theta = \theta_{\max}}, \quad (8)$$

$$\phi_{\mathrm{src}}^{\max,>} = \frac{2\pi\nu - (\alpha_{\mathrm{img}} - \alpha_0) - 2\phi_0\chi_{\mathrm{act}}}{4\chi_{\mathrm{act}}} \Big|_{\theta = \theta_{\max}}$$
$$\cdot \left\{ 1 \pm \sqrt{1 + \frac{8\chi_{\mathrm{act}}[2 - \phi_0\chi_{\mathrm{DR}}(\alpha_{\mathrm{img}} - \alpha_0 - 2\pi\nu)]}{\chi_{\mathrm{DR}}(2\pi\nu - (\alpha_{\mathrm{img}} - \alpha_0) - 2\phi_0\chi_{\mathrm{act}})^2}} \right\}. \quad (9)$$

The expressions in Eqs. (7)–(9) establish the desirable analytical relation between the recombination zone location, $z' = \phi_{\mathrm{src}}/k_1$, and the angles in which the emission pattern extrema occur. Equation (7) is applicable for angles in which a local minimum of the emission pattern occurs, and Eqs. (8) and (9) are applicable for angles in which a local maximum occurs. The solution $\phi_{\mathrm{src}}^{\max,<}$ is valid whenever $|(\phi_{\mathrm{src}}^{\max,<} + \phi_0)\chi_{\mathrm{DR}}| \leq 1$, whereas the solution $\phi_{\mathrm{src}}^{\max,>}$ is valid whenever $|(\phi_{\mathrm{src}}^{\max,>} + \phi_0)\chi_{\mathrm{DR}}| \geq 1$. If both conditions are met simultaneously, then the most accurate solution is given by $\bar{\phi}_{\mathrm{src}}^{\max} = \frac{1}{2}(\phi_{\mathrm{src}}^{\max,<} + \phi_{\mathrm{src}}^{\max,>})$.

We verify our results using the prototype device (Fig. 1) based on the device analyzed, fabricated, and measured by Mladenovski *et al.* [3]. The device configuration can be matched to the one presented in Fig. 1 herein, with $n_{-2} = 0.129$, $n_1 = 1.8$, $n_3 = 1.5$, $n_4 = 1$ as the refractive indices of the organic layers, glass substrate, and air region, respectively, and the extinction coefficient of the silver
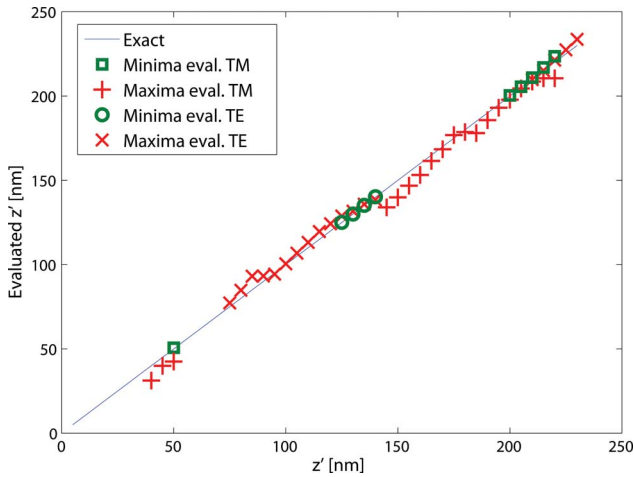
Fig. 2. (Color online) Comparison of the exact recombination zone location (blue line) with the values extracted from the emission pattern local minima (green circles and squares) and local maxima (red × and + symbols) produced by electric (circles and × symbols) and magnetic (squares and + symbols) line sources located in position z'.

cathode set to $\kappa_{-2} = 3.25$. The emission central wavelength is $\lambda = 530$ nm, and z' can get values up to 230 nm. A comparison between the exact source locations and the evaluated recombination zone from simulated emission pattern minima and maxima, for both electric and magnetic line sources, is presented in Fig. 2. The evaluation is performed using Eqs. (7)–(9) with $\nu = 0$ for $z' \lesssim \frac{1}{2}\lambda/n_1$ and $\nu = 1$ for higher values. Values of z', for which no evaluation is available on the plot, are emitter locations for which the emission pattern has no extrema except for $\theta = 0$.

Figure 2 shows a good agreement between the extracted recombination zone locations and the exact values, for both electric and magnetic line source emission patterns. Moreover, it is observed that for almost all of the relevant range of emitter position values, at least one of the polarization sources produces extrema that allow the desired extraction.

To demonstrate the efficiency and accuracy of the method, we extract the recombination zone location from the measured emission patterns presented in Fig. 4 of [3]. The device configuration dictates that $r_{\mathrm{img}} = 0.55$, $r_{\mathrm{act}} = 5/6$, $r_{\mathrm{sub}} = 1$, and $\phi_{\mathrm{src}} = z'[\mathrm{nm}]/46.86$. For the emission pattern plotted in Fig. 4(c) of [3], we identify a local maximum around $\theta = \pi/6$. Calculating the angle-dependent parameters from Eqs. (7)–(9) for this value, we find that $\chi_{\mathrm{DR}} = 4.272$, $\chi_{\mathrm{act}} = 0.909$, $\alpha_{\mathrm{img}} = 0.933$, and $\phi_0 = 0.442$ for the TE case. Using $\nu = 1$, we arrive at $\phi_{\mathrm{src}}^{\mathrm{max},<} = 0.758$ and $\phi_{\mathrm{src}}^{\mathrm{max},>} = 4.719$. This implies that $|(\phi_{\mathrm{src}}^{\mathrm{max},<} + \phi_0)\chi_{\mathrm{DR}}| > 1$ and $|(\phi_{\mathrm{src}}^{\mathrm{max},>} + \phi_0)\chi_{\mathrm{DR}}| \geq 1$. Hence,

according to the method described above, only the second solution is valid; it yields $z' = 221$ nm. The distance of the recombination zone from the cathode was designed by Mladenovski *et al.* [3] to be 230 nm for the case considered, and it is readily observed that the results obtained by the method presented in this Letter are in good agreement with this value. The same procedure can be performed for the emission pattern presented in Fig. 4(b) of [3], and a similar agreement between the extracted values and the listed values is found when the local maximum in $\theta = \pi/3$ and $\nu = 0$ is used for the evaluation process. The method is proved to work well for other sets of materials as well, e.g., when executed on the results presented in Fig. 2 of [6]. From these results, we conclude that the TE polarization is dominant in the devices measured in [3,6], and that there is considerable similarity between the results obtained by the simplified 2D models and of the realistic 3D models, at least as far as emission patterns are concerned.

To conclude, we have presented an analytical method for extracting electrical properties of OLEDs, namely, the recombination zone location, from measured optical characteristics, namely the emission pattern extrema they produce. This method was applied to a prototype device, and very good agreement between measured and extracted values was demonstrated. These results emphasize the importance of analytical approaches for optical analyses of OLEDs, leading to a clear physical interpretation of the dominant processes in the device as well as simple and powerful analytic tools, which can be efficiently utilized by engineers for device optimization and design verification.

References

1. R. H. Friend, R. W. Gymer, A. B. Holmes, J. H. Burroughes, R. N. Marks, C. Taliani, D. D. C. Bradley, D. A. D. Santos, J. L. Bredas, M. Logdlund, and W. R. Salaneck, Nature **397**, 121 (1999).
2. N. Tessler, G. J. Denton, and R. H. Friend, Nature **382**, 695 (1996).
3. S. Mladenovski, K. Neyts, D. Pavicic, A. Werner, and C. Rothe, Opt. Express **17**, 7562 (2009).
4. M. Slootsky and S. R. Forrest, Opt. Lett. **35**, 1052 (2010).
5. C.-L. Lin, T.-Y. Cho, C.-H. Chang, and C.-C. Wu, Appl. Phys. Lett. **88**, 081114 (2006).
6. J. Lee, N. Chopra, and F. So, Appl. Phys. Lett. **92**, 033303 (2008).
7. N. Tessler, Appl. Phys. Lett. **77**, 1897 (2000).
8. T. Granlund, L. A. A. Pettersson, and O. Inganas, J. Appl. Phys. **89**, 5897 (2001).
9. B. Ruhstaller, T. Beierlein, H. Riel, S. Karg, J. Scott, and W. Riess, IEEE J. Sel. Top. Quantum Electron. **9**, 723 (2003).
10. A. Epstein, N. Tessler, and P. D. Einziger, IEEE J. Quantum Electron. **46**, 1388 (2010).